RSC Advances

ROYAL SOCIETY OF CHEMISTRY

www.rsc.org/advances

Journal Name

ARTICLE

Stacked $Cu_{1.8}S$ nano platelets as Counter Electrode for Quantum Dot Sensitized Solar Cell

Received 00th January 20xx,
Accepted 00th January 20xx

DOI: 10.1039/x0xx00000x

www.rsc.org/

A. Dennyson Savariraj,[a] G. Rajendrakumar,[a] Samayanan Selvam,[a] S.N.Karthick, B.Balamuralitharan,[a] Hee-Je Kim,[a] Kodakkal Kannan Viswanathan,[b] M. Vijaykumar Kandasamy Prabakar [a*]

It is found that electrocatalytic activity of $Cu_{2-x}S$ thin films used in quantum dots sensitized solar cells (QDSSC) as counter electrode (CE) for the reduction of polysulfide electrolyte depends on the surface active sulfide and disulfide species and deficiency of Cu. The preferential bonding between Cu^{2+} and S^{2-} leading to the selective formation of $Cu_{1.8}S$ stacked platelets like morphology is determined by Cetyl Trimethyl Ammonium Bromide surfactant with temperature and crab Cu-S coordination bond formed dictates the surface area to volume ratio of the $Cu_{1.8}S$ thin films and the electrocatalytic activity. The Cu deficiency enhances the conductivity of the $Cu_{1.8}S$ thin films and exhibits near- infrared localized surface plasmon resonance due to free carriers and UV-VIS absorption spectra shows excitonic effect due to quantum size effect. When these $Cu_{1.8}S$ thin films were employed as CE in QDSSC, robust photoconversion efficiency of 5.2 % is yielded for the film deposited at 60 ˚C by a sinlge step chemical bath deposition method.

1.Introduction

Quantum dot sensitized solar cells (QDSSC) emerged as an alternative to dye sensitized solar cells (DSSC) which failed due to photo degradation in spite of being cost effective.[1] To overcome this, inorganic quantum dots (QDs) are used as photosensitizer due to generation of multiple excitons through impact ionization with single photon absorption in addition to band gap tunability.[2-4] QDs incorporated in to the photoanode absorb incident light over a wide range of spectral wavelength with flexible tandem arrangement.[1,5] Even though, QDSSCs outperform organo metallic dye based DSSCs in terms of stability against photo degradation, the photovoltaic performance is still very low.[6-9] Many efforts have been made to improve the efficiency by employing cascade layers of FTO/TiO_2 with different QDs such as PbS,[10] CdS,[11] CdSe,[12] and CdS/CdSe hetero structures [13] as efficient sensitizers in QDSSCs with enhanced charge separation due to large intrinsic dipole moment.[13] In QDSSC, counter electrode (CE) is an equally important component since it plays crucial role of electrolyte reduction. In comparison to several CEs, platinum (Pt) has both high electrocatalytic activity and very low resistance for the iodide/triiodide redox electrolyte reduction when employed in DSSC [14] however, failed to perform well in QDSSC with sulfide/polysulfide (S^{2-}/S_n^{2-}) redox couple electrolyte since it readily adsorbs S^{2-} on to the surface which increase the sheet resistance and hence electrocatalytic activity is reduced.[15,16] In this regards, it is highly essential to find a suitable CE which can alleviate afore mentioned problem with concurrent improvement in efficiency of the solar cells since the regeneration rate of the QDs depends on the redox rate of the electrolyte.[17] In view of this, several materials have been employed as an alternative CE, right from carbon based candidates like carbon nano tubes[18] to transition metal sulphides.[19-21] The carbon based materials lack either catalytic activity or effective charge conduction even though they provide large surface and uniform pores.[22] Among metal sulfides, group IB-VIA metal chalcogenides (MC) $Cu_{2-x}S$ is found to be a well suited CE due to its self-doped p-type semiconducting nature with tunable phase and surface morphologies depending on the preparation method.[23] The surface morphology and chemical species present at surface are often the finger prints of the material's properties to suit the need and more specifically the electrocatalytic properties of $Cu_{2-x}S$ nanostructures.[24] Therefore, synthesizing $Cu_{2-x}S$ with tailored properties becomes both inevitable and challenging towards high photoconversion efficiency of QDSSCs [25]. In order to synthesize of such well-defined structures, bottom up

[a] Department of Electrical and Computer Engineering, Pusan National University, San 30, Jangjeong-Dong, Gumjeong-Ku, Busan-609 735, South Korea.
[b] UTM Centre for Industrial and Applied Mathematics, Department of Mathematical Sciences, Universiti Teknologi Malaysia, 81310, Johor Bahru, Johor, Malaysia.
[c] Pacific Northwest National Laboratory (PNNL), Richland, WA-99354, USA

† Footnotes relating to the title and/or authors should appear here.
Electronic Supplementary Information (ESI) available: [details of any supplementary information available should be included here]. See DOI: 10.1039/x0xx00000x

process with controlled nucleation is very handy. Therefore, several experimental parameters such as concentration, temperature, reaction time and concentration of surfactants or capping agents or structure- directing agent (SDA) are to be fine-tuned to obtain both size and shape controlled $Cu_{2-x}S$ nanostructures [24]. Cetyl Trimethyl Ammonium Bromide (CTAB) is one such SDA that binds well with the $Cu_{2-x}S$ coordination formed in the initial stage and as the reaction proceeds it determines the shape and morphology of the $Cu_{2-x}S$ thin films to be synthesized.

Moreover, it is essential to optimize the molarity, quantity of precursor solutions, temperature and position of substrate inside the growth vial in order to assure quality of the films grown by chemical bath deposition (CBD) methods. Growth of $Cu_{2-x}S$ thin film was not initiated below 55 ˚C and the deposited films peeled off from the substrate above 65 ˚C. The $Cu_{2-x}S$ thin films grown at optimized temperature were characterized like phase, composition, surface morphology and electrochemical properties associated with QDSSC. We strongly believe that our method is very simple and the clearly demonstrated growth method would allow the researchers to further tailor the properties of $Cu_{2-x}S$ thin films to suit their needs. In this report, we have presented one step CTAB assisted synthetic route to fabricate stacked nano platelets like $Cu_{2-x}S$ thin films using simple chemical bath deposition (CBD) by varying the deposition temperature for a period of 2 hours. It is found that both temperature and SDA influence the shape and surface morphology. The $Cu_{2-x}S$ thin films synthesized possess stacked nano platelets like structure with large surface to volume ratio terminated with different surface active sulfide, disulfides and oxides. This in turn influences their electrocatalytic activity and particularly enhances the redox reaction of sulfide/polysulfide (S^{2-}/S_n^{2-}) redox couple electrolyte when the $Cu_{2-x}S$ thin films are employed as CE for QDSSCs. The QDSSC fabricated using $Cu_{2-x}S$ thin film synthesized at 60 °C giving a photo conversion efficiency of up to 5.2 % with consistent stability. Based on X-ray photoelectron spectroscopy (XPS), impedance spectroscopy and Tafel polarization, a detailed exploratory investigation of the electrocatalytic behavior of the CE is discussed and presented here.

2. Experimental

2.1 Materials

$Cu_{2-x}S$ of stacked nano platelets were successfully deposited by CBD using water as solvent on well cleaned fluorine doped tin oxide (FTO) of resistance 7 Ω/cm^2 (Hartford Glass). All the precursors used for the synthesis were analytical grade and purchased from Sigma Aldrich and the synthesis was carried out without further purification.

2.2 Preparation of photo anode and counter electrode

The typical synthesis was carried out by dissolving 0.1 M of copper chloride ($CuCl_2.2H_2O$) in 50 ml of deionized water and 1.0 M of thioacetamide (CH_3CSNH_2) was added for S source followed by adding 1.1 M of acetic acid (CH_3COOH) in drops and stirred continuously. To the above solution, 0.013 M of CTAB (($C_{16}H_{33}$) N (CH_3)$_3$Br) was added and stirred vigorously for 25 minutes to make a homogeneous solution. The previously cleaned FTO glass substrates were immersed and kept horizontally in to the growth solution and chemical bath deposition was carried out for 2 hours at 55 °C, 60 °C and 65 °C and the samples were labelled CE55, CE60 and CE65 respectively. Above 65 °C, the deposited $Cu_{2-x}S$ films were peeled off from the substrate and hence not suitable for CE. The CBD synthesized stacked $Cu_{2-x}S$ nanoplatelts were then rinsed with deionized water and 99% ethanol and purged with N_2 gas.

The photoanodes were prepared by coating commercially available TiO_2 paste of particle size 20 nm (Ti-Nanoxide HT/SP, Solaronix) on the FTO using doctor blade method and were sintered at 450 °C for 30 minutes to evaporate the solvents. The QDs photosensitizers were coated on the TiO_2 using successive ionic layer adsorption and reaction method (SILAR) with optimized conditions already reported elsewhere[26]. For CdS quantum dots, 0.025 M cadmium acetate dihydrate (Cd (CH_3COO)$_2$. $2H_2O$ and 0.2M sodium sulfide (Na_2S) were prepared in 50 ml of deionized water separately for cation and anion sources respectively and 5 cycles of SILAR were carried out. For CdSe QDs, the cation sources was prepared by dissolving 0.025 M of (Cd (CH_3COO)$_2$. $2H_2O$) in 50 ml of deionized water. The anion source containing Se was prepared by from aqueous 0.2 M selenium (Se) and 0.4 M (Na_2SO_3) taken in a round bottom flask. This solution was refluxed at 125 ˚C for a period of two hours to get sodium selenosulfate (Na_2SeSO_3) as selenium is not soluble in water and cannot react in pristine form. Using the above prepared cation and the anion precursors, 8 SILAR cycles of CdSe QDs was deposited, while the temperature of the precursors are kept 55 ˚C for better adsorption. Finally, to avoid corrosion due to the polysulfide electrolyte and back electron transfer into electrolyte, two SILAR cycles of zinc sulfide (ZnS) passivation layer was coated using 0.2 M of zinc nitrate hexahydrate ($ZnNO_3$. $6H_2O$) and 0.2 M of Na_2S solutions.

2.3 Fabrication of QDSSCs and Symmetric cells

The QDSSCs were assembled by sandwiching the SILAR processed tandem layered TiO_2/CdS/CdSe/ZnS photoanodes and chemical bath deposited $Cu_{2-x}S$ and Pt CEs with a 25µm hot-melt sealing sheet (SX 1170-25,Solaronix) in between them. The set up was heated at 110 °C in a hotplate for 45 seconds. Then, the internal space of the cell was filled with the sulfide/polysulfide (S^{2-}/S_n^{2-}) redox couple electrolyte comprising of 1M of Na_2S, 2M of S and 0.2M of KCl by capillary action. In the case of symmetric cells, the photoanode was replaced with CE itself such as $Cu_{2-x}S$/sulfide-polysulfide (S^{2-}/S_n^{2-})/ $Cu_{2-x}S$ and Pt in place of $Cu_{2-x}S$ served as reference were

sandwiched by a 25 µm hot-melt sealing sheet and the space between them were filled with polysulfide electrolyte.

2.4. Characterizations

The phase purity and crystallinity of $Cu_{2-x}S$ thin films were analyzed using X-ray diffraction (XRD; Bruker D8-Advance) with Cu Kα radiation (λ =1.54056) source operated at 40 kV and 30 mA in the range of 10 – 80˚. The surface morphology of the thin films was analyzed using (FE-SEM Hitachi, Model SU-70). UV-Vis spectroscopic analysis was carried out using optizen 3220 UV. X-ray photon spectroscopy (XPS) was performed using a VG scientific ESCALAB250 with monochromatic Al-Kα radiation of 1486.6 eV with an electron take off angle of 90˚. The survey spectrum was scanned in the binding energy (BE) range of 0.0 - 1400 eV in steps of 1 eV. The binding energy values reported here is relative to the carbon C 1s core level at 284.6 eV. The pressure of the chamber was maintained at 10^{-10} torr throughout the measurement. The current-voltage characteristic of the QDSSCs were studied under 1 sun illumination (AM 1.5G 100m Wcm^{-2}) with san Ei Electric (XES 301S, Japan) solar simulator having the irradiance uniformity of ±3%. Electrochemical impedance spectroscopy (EIS) was performed using a BioLogic potentiostat/galvanostat/EIS analyzer (SP-150, France) under 1 sun illumination.

3. Result and Discussion

3.1 XRD- Analysis

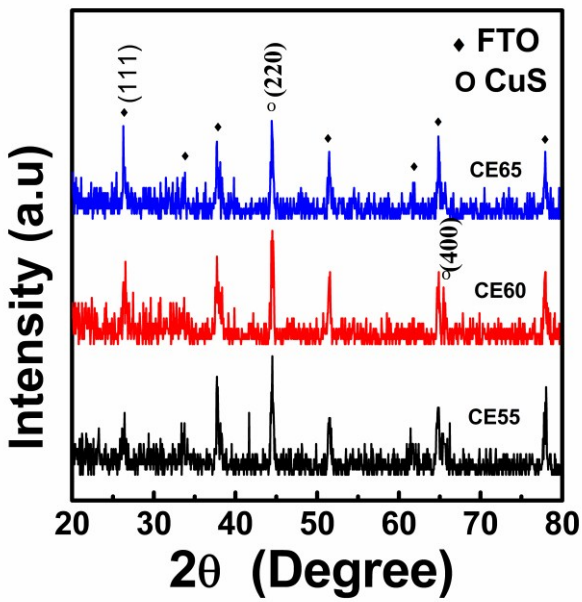

Figure 1 represents the X-ray diffraction pattern of CBD deposited $Cu_{2-x}S$ thin films on FTO substrate.

The diffracted peaks of all the films are found to be along (111), (200), (220), (400) and (313) planes corresponding to 26.465, 31.175, 44.125, 65.479 and 70.741 2θ values matching cubic phase of $Cu_{1.8}S$ (ICDD file No. 01-075-2241).

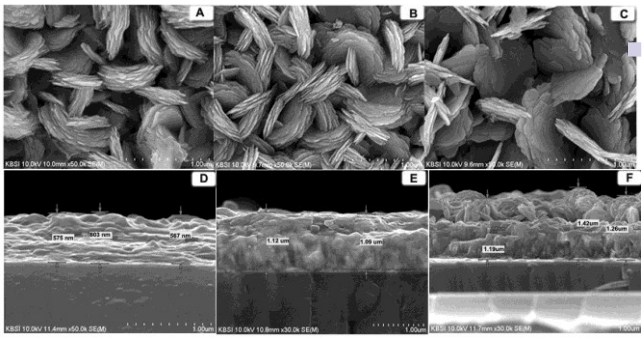

Figure2. The SEM images of stacked Cu1.8S nanoplatelets (a) CE55 (b) CE60 (C) CE65 deposited on FTO substrates.

In the case of $Cu_{2-x}S$, identifying and attributing the correct phase is difficult since there exists many phases for the bulk $Cu_{2-x}S$ with its composition close to the ratio of Cu/S =2; like anilite, chalcocite, digenite, djurleite, which all have the maximum intensity diffraction peak at 46 degree of 2θ value. However, in our case it is easy to identify the phase since; the diffraction plane at 44.5 degree occurs only for cubic phase of $Cu_{1.8}S$ and hence referred here after instead of $Cu_{2-x}S$. The grain sizes were calculated from Scherer's method and are 112, 167 and 152 respectively for CE 55, CE60 and CE 63. The slight decrease in grain size for CE65 might be due to the reduced thickness of the nano platlets. The intensity of the diffraction plane <111> increases with increase in deposition temperature while <400> plane appears for CE 60. Even though, there is not much remarkable changes in the phase the $Cu_{2-x}S$ thin films, little changes in orientation of the nano platlets might have caused the disappearance of <400>plane for CE65 and is evidenced from the SEM images.

3.2 Surface morphological studies and growth mechanism

Figure 2 (a), (b) and (c) show the SEM images of the $Cu_{1.8}S$ thin films deposited at 55 °C (CE55), 60 °C (CE60) and 65 °C (CE65) respectively while Figure 2 (d), (e) and (f) display the cross section of the respective films. The surface of the CE55 exhibits uniform arrangement of stacked nano platelets with less density while raising the deposition temperature to 60 °C gives evenly distributed $Cu_{1.8}S$ of dense nano platelet with increased surface area to volume ratio. However, the surface morphology of the film deposited at 65 °C shows nano platelets with reduced thickness. The uniform surface morphology and high crystallinity of the $Cu_{1.8}S$ is greatly influenced by CTAB, which allows the system to bypass self-agglomeration and provides capping and surface transformation to the $Cu_{1.8}S$ nanoplatelets. CTAB is basically a strong cationic surfactant which can form micelles in the solution. Based on the solution conditions, CTAB forms

micelles of different shapes like cylindrical, spherical, high order lamellar to give crystals of different shapes[27]. The S^{2-} ions generated through the hydrolysis of thioacetamide are readily attracted by Cu^{2+} ions and form a crab like Cu-S coordination bond [26]. The supply of S^{2-} ion is enhanced by acetic acid which also acts as a stabilizing agent. When cationic CTAB is introduced, it forms a micelle and is attracted by S atoms present in the $Cu_{1.8}S$. Apart from the prevention of self - agglomeration by CTAB, π-π bond interactions and weak Van der Waals attraction directs the reaction towards the formation of stable $Cu_{1.8}S$ nano platelets (Figure 3)[28, 29]. The preferential bonding between Cu^{2+} and S^{2-} leads to the selective formation of $Cu_{1.8}S$. Due to the three dimensional surface of the thin films, the thickness of the films vary from place to place as revealed in the cross section of the film as seen in Figure 2 (d), (e) and (f).

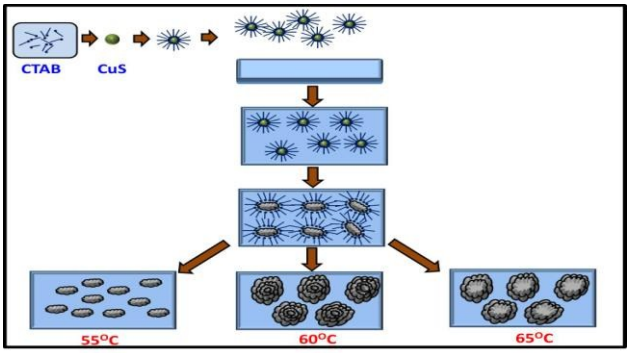

Figure 3. The schematic of CTAB assisted Cu1.8S stacked nanoplatelets formation on FTO substrates.

3.3 Optical Studies

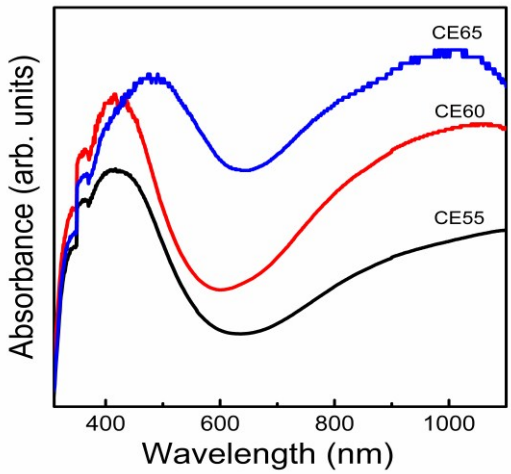

Figure 4. UV absorption spectra of stacked $Cu_{1.8}S$ nanoplatelets deposited on FTO substrates.

Figure 4 compares the absorption spectra of the $Cu_{1.8}S$ thin films fabricated via CBD. All the films show absorption at UV/visible region and is red shifted as the deposition temperature is increased due to quantum confined exciton effect and the absorption in NIR regions corresponds to localized surface plasmon resonance (LSPR) due to free carrier density.

This is due to the presences of free holes (Cu vacancy) in the valance band that can act as self-dopants leadin to resonance absorption[23]. The absorption maximum in the UV/VIS is at 410, 417 and 475 nm respectively for CE55, CE60, CE65 samples with increased absorption. These high energy absorption peaks arises from the 1Sh - 1Se Figure 3. The schematic of CTAB assisted Cu1.8S stacked nanoplatelets formation on FTO substrates.excitonic transition found in semiconductor nanoparticles[30]. From the absorption spectrum, the band gaps of the $Cu_{1.8}S$ thin films were calculated to be 2.2, 2.1 and 1.75 eV respectively for CE55, CD60, CE65. The reduction in the band gap is due to the formation of uniform crystals of increased size showing quantum confinement effect. On the longer wavelength region, non-stoichiometric $Cu_{1.8}S$ (x > 0) develops an LSPR in the NIR region and shifts to blue region with strong absorption due to higher free carrier come from increased copper vacancies.[32] The LSPR properties are always influenced by the surrounding medium and increase of the refractive index red shifts the NIR absorption of NCs. Here, the $Cu_{1.8}S$ films synthesized exhibit significant LSPR features with only air as the surrounding medium and hence the blue shift might come from the Cu deficiency [23,33,34]. The absorption of light in the NIR spectral window is also suitable to harvest the residual light penetrated from the tandem layered photoanode. This p-type semiconductor material can also contribute to the increase of the photo voltage with its photoactive nature through the auxiliary tandem junction[1].

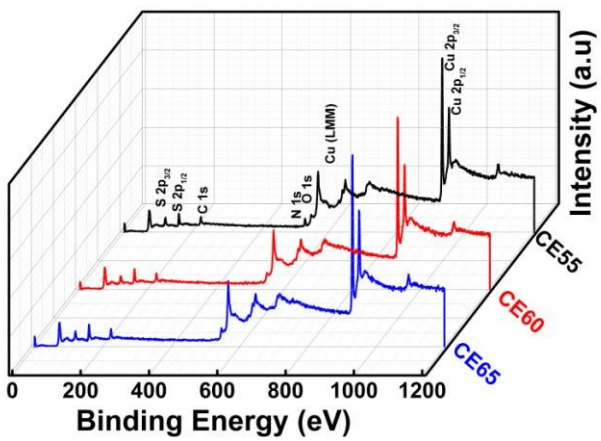

Figure 5. XPS survey spectra of $Cu_{1.8}S$ stacked nanoplatelets deposited on FTO substrates.

3.4 XPS- Analysis

The XPS analysis was utilized to infer the ionization states, elemental composition and to ensure the purity of the $Cu_{1.8}S$ thin films compounds. The samples were not subjected to any pre or post heat treatment. The presence of Cu, S, C and O elements are confirmed from the XPS survey spectrum presented in Figure 5. From the Auger line of Cu LMM at the binding energy of 569.0 eV, the presence of bivalent Cu is evidenced. The atomic % of Cu:S:O were 54.62:34.86:10.52, 62.18.36.3:1.45, 60.18:35.96:3.86 respectively for CE55, CE60 and CE65. CE55 shows very low S content due to slow sulfidation rate at low temperature and has more oxygen. On the other hand, both CE60 and CD65 have almost equal atomic % of S. In order to elucidate the nature of bonding of the surface elements, the individual core level spectra of S2p and Cu_{2p} were measured at higher rate of resolution. XPS data were fitted with Gaussian-Lorentzian (30 % Gaussian) functions and Shirley type background using Casa XPS Software. Four constraints were applied to fit S peak components such as the spin orbit splitting (1.18 eV between $2P_{3/2}$ and $2P_{½}$), the peak area ratio ($2P_{3/2}$: $2P_{1/2}$ = 2:1), equal full width at half maximum and the binding energy positon of S $2P_{3/2}$ was fixed at 161.2 eV. Figure 6 represents the individual S_{2p} peaks with clear distinction of their bonding whereas Cu does not show remarkable changes in the oxidation state and all spectra have satellite peaks due to Cu vacancy which have caused the LSPR in the optical spectra.[23]

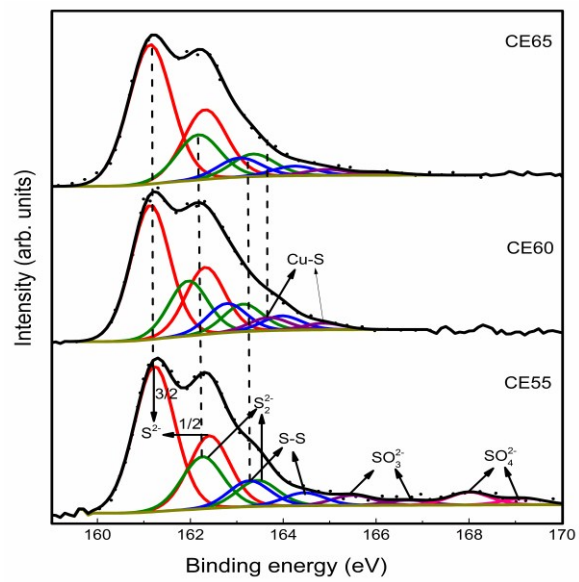

Figure 6. XPS spectra for S2p of $Cu_{1.8}S$ nanoplatelets.

The S_{2p} (S^{2-}) doublet peaks (161.2 and 162.38 eV) of $Cu_{1.8}S$ is attributed to the presence of $S_{2p3/2}$ and $S_{2p1/2}$ states. CE55 has both sulfide (SO_3^{2-}) and sulfates (SO_4^{2-}) respectively at 165.5 and 168 eV at the surface and are absent in CE60 and CE65. This clearly shows that oxidation is much higher for low S content samples prepared at low temperature. The peak found at 163.3 is assigned to bridging sulfur (S-S) which is at lower binding energy state (less oxidation) in CE60, however, has Cu-S, disulfide (S_2^{2-}) and sulfide (S^{2-}) peaks at 163.7, 162 and 161.2, respectively.[35,36]. The presence of S in the form of SO_4^{2-} at surface of the films is in a residual form which is further confirmed from O1s peak located at 532.2eV in the survey spectrum[37]. These clearly show that the surface bonding is controlled by the temperature.

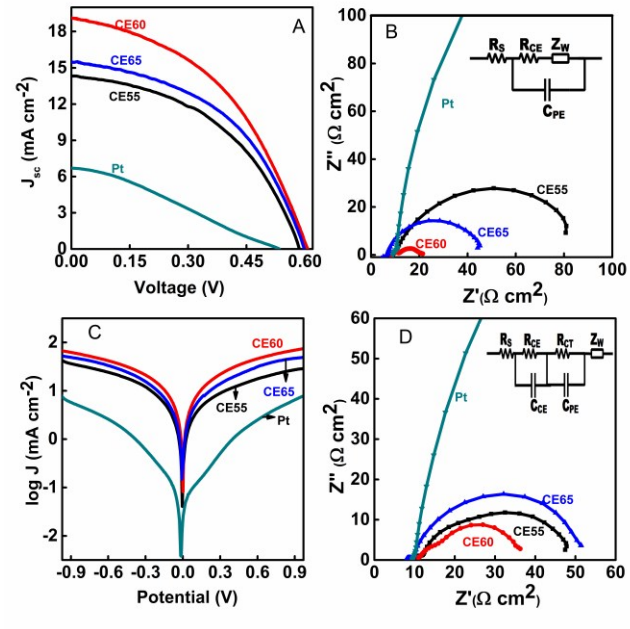

Figure 7. (a) I-V behavior for TiO_2/CdS/CdSe/ZnS QDSSCs based on stacked $Cu_{1.8}S$ nanoplatelets and Pt counter electrodes. (b) Nyquist plot for $Cu_{1.8}S$ and Pt symmetrical cells: Inset shows equivalent circuit. (c) Tafel polarization plot for $Cu_{1.8}S$ and Pt symmetrical cells. (d) Nyquist plot of TiO_2/CdS/CdSe/ZnS QDSSCs for $Cu_{1.8}S$ and Pt counter electrodes. Inset shows the equivalent circuit.

3.5 IV Characteristics and Electrochemical Characterizations

Figure 7 (a) shows the J-V characteristics of the QDSSCs fabricated with TiO_2/CdS/CdSe/ZnS as the photoanode and CBD synthesized $Cu_{1.8}S$ and Pt (reference) as CE and polysulfide as electrolyte. The photovoltaic parameters are summarized in Table 1. The best photo conversion behavior is observed for CE60 with Voc = 0.606 V, JSC = 19.079 mA/cm^{-2}, FF = 45.05 and η = 5.16 % and Pt CE shows Voc = 0.559 V,JSC = 6.671 mA/cm^{-2}, FF = 31.71 and η = 1.45%. The affinity of Pt CE towards S^{2-} accounts for its poor performance, which slows down the electrocatalytic activity of Pt with a rapid decrease in the current density and fails to reduce the redox electrolyte on its surface.[38,39] All the $Cu_{1.8}S$ CEs give better performance than Pt and among the $Cu_{1.8}S$ CEs, the performance of CE60 is better than the rest. The surface active S species are very crucial for the electrolyte reduction. However, bridging S-S is more resistive than Cu-S bond presence in CE 60. Hence, the improvement might have come from the surface active species in addition to the surface morphology influenced by CTAB which plays a role of structure directing agent to improve the shape and surface morphology and in turn the photo conversion ability. The stacked platelets like structure

possesses increased surface to volume ratio that provides larger area of contact for the electrolyte. The interfaces between the stacked layers too offer space for the electrolyte to flow. Therefore the redox reaction of the electrolyte is enhanced. Even though, efficiency is much higher than the earlier reports,[23,26] the FF is much lower which might be due to higher charge transfer resistance (R_{CT}) of the QDSSC.

The scavenging attitude of the sulfide ions (S^{2-}) over the photogenerated holes at the photo anode and the oxidized ions (S_x^{2-}) to reach the CE in order to combine with the electron, must be enhanced by the CE.[1]
Therefore, the charge transfer resistance (R_{CT}) of the QDSSC, which determines the electrocatalytic activity of the counter electrode has to be studied by using electrochemical impedance spectroscopy (EIS). Figure 7(b) shows the Nyquist plots of the symmetrical cells and the equivalent circuit (inset) is made with a series resistance (Rs) which represents a high-frequency non zero intercepts on the real axis, the resistance at the counter electrode electrolyte interface (R_{CE}) and the respective capacitance (C_{PE}) with the diffusion impedance (Z_W) represented by a saturated semicircle usually observed at the low frequency. The symmetrical cells were made of two identical $Cu_{1.8}S$ and Pt CEs respectively with an active area of 1 cm^2 and the polysulfide electrode in between them. The measurements were carried out in the frequency range of 0.1 Hz - 500 kHz. The obtained impedance data were fitted using the equivalent circuit given in the inset and the parameters extracted are presented in table1. The value of R_s for the $Cu_{1.8}S$ CEs decreases as the deposition temperature is increased indicating better adhesion of the $Cu_{1.8}S$ thin films on to the FTO substrate. The extent of R_{CE} determines the charge transfer between the CE and the electrolyte towards the redox reaction of S^{2-}/S_n^{2-}. It is found that Pt CE has highest R_{CE} value of 576.23 Ω against the very small values for $Cu_{1.8}S$ CEs, and among $Cu_{1.8}S$ CEs, CE60 has the lowest value of 3.26 Ω while CE55 and CE65 have larger R_{CE} values than CE 60 and therefore this accounts for the enhanced performance of CE60. The diffusion impedance (Z_W) is yet another yardstick to determine the ability of a CE in reducing the redox polysulfide electrolyte. Pt CE has the highest value of 102.58 Ω suggesting poor ability and strong resistance to reduce the electrolyte as catalytic poisoning hinters.[40,41] On the contrary, the $Cu_{1.8}S$ CE with very negligible values outperform Pt CE (CE55 = 1.49 Ω, CE60 = 0.34 Ω and CE 65 = 0.76 Ω (Not shown in the table).

In order throw light on the better electrocatalytic activity and the interfacial charge transfer property of S^{2-}/S_n^{2-} redox couple Tafel polarization measurement was carried out using the symmetrical cells. Figure 7 (c) shows the logarithmic current density (log J) as a function of Voltage (V) for the redox reaction of polysulfide electrolyte redox couple (S^{2-}/S_n^{2-}). By extrapolating the linear region of the curve towards the zero over potential and from the intercept, the exchange current density (J_0) was obtained. The exchange current density (J_0) and limiting current density (J_{lim}) determine electrochemical activity of the CE. As seen in Figure 7 (c), except Pt all the CEs show almost even anodic and cathodic slopes. CE60 shows a higher slope both on anodic and cathodic side with zero corrosion potential. Its highest limiting current density (J_{lim}), highest corrosion current of 3245.61 µA and balanced oxidation and reduction rate is confirmed from its equal cathodic (βc) (298.0 mV) and anodic slopes (βa) (300.1 mV) further support its best performance, yielding an efficiency of 5.16%. CE55 and CE65 stay behind CE60 with lower corrosion current (I_{corr}) of 2778.95 µA and 2285.68 µA respectively. CE 65 has slightly predominant cathodic slope (βc) (299.7mV) over that of anodic slope (βa) (286.4mV) with corrosion potential of (E_{corr}) -1.843mV and therefore a slight shift from the equilibrium reduces their catalytic activity. CE 55 with lowest limiting current density (J_{lim}) and high corrosion potential (E_{corr}) of -7.512mV becomes the least performing counter electrode. In addition to that uneven cathodic and anodic slopes also (βc = 283.4mV, βa = 310.6 mV) make it inferior among the $Cu_{1.8}S$ counter electrodes. In the case of Pt CE, it not only has uneven cathodic and anodic slopes, (βc = 290.00mV, βa = 330.2mV) and lowest limiting current density (J_{lim}), but also has negative corrosion potential (E_{corr}) of -18.16 mV. Pt CE'S large negative corrosion potential (E_{corr}) means that when all the $Cu_{1.8}S$CEs can readily reduce the polysulfide electrolyte Pt CE has to attain equilibrium (null point) prior to its commencement of reduction of polysulfide electrolyte at

Table 1 Photovoltaic and Electrochemical impedance spectroscopic parameters of QDSSCs

Cell	Composition Cu:S (atomic %)	EIS for symmetric cell		Voc (V)	Jsc (mA/cm^2)	FF (%)	η (%)	EIS parameters for QDSSCs			
		Rs (Ω)	R_{CE} (Ω)					Rs (Ω)	R_{CE} (Ω)	R_{CT} (Ω)	Z_W (Ω)
55°C	52.12:47.88	8.71	71.91	0.58	14.3	46.15	3.84	9.39	2.13	36.13	1.61
60°C	51.93:48.07	8.26	3.26	0.60	19.1	45.05	5.16	9.22	1.7	24.19	1.17
65°C	51.60:48.40	6.44	38.69	0.59	15.4	47.07	4.28	7.86	1.39	41.50	2.10
Pt		8.83	576.23	0.56	06.7	31.71	1.19	9.86	12.32	418.47	10.24

the expense of photoconversion ability.[20] To support the above said reasons for the better electrocatalytic activity of CE60, the internal charge transfer kinetics must be explained from EIS point of view. The EIS measurements for the QDSSCs were carried out at open circuit voltage (V_{OC}) (light condition). The impedance data were fitted using the equivalent circuit given in the inset in Figure 7 (d). In the circuit R_{CE} represents electron transfer at the counter electrode/polysulfide electrolyte interface, R_{CT} represents charge transfer resistance at the photoanode/polysulfide electrolyte interface and C_{PE} is the chemical capacitance related to amount of photoexcited charge carriers available in the conduction band of the photoanode which result from minimum recombination and Z_W is the diffusion resistance. The QDSSC assembled with CE60 gives an R_{CE} of 1.7 Ω and Z_W = 1.17 Ω showing better reduction rate of the electrolyte and electrolyte diffusion. On the contrary Pt CE with a high R_{CE} = 12.32 Ω and Z_W = 10.24 Ω as it is subjected to adsorption of S^{2-} makes it poor to reduce the electrolyte with the supply of electron. Therefore, Pt CE fails to have better photoconversion ability and reduced FF, while all the $Cu_{1.8}S$ CEs have high J_{SC} and photo conversion ability. The best photoconversion efficiency demonstrated by CE60 is due to i) have low resistance and ii) have zero corrosion potential implies that the system is already at equilibrium to readily reduce the electrolyte unlike Pt whose negative corrosion potential must be balanced with additional sacrifice of energy.[42]

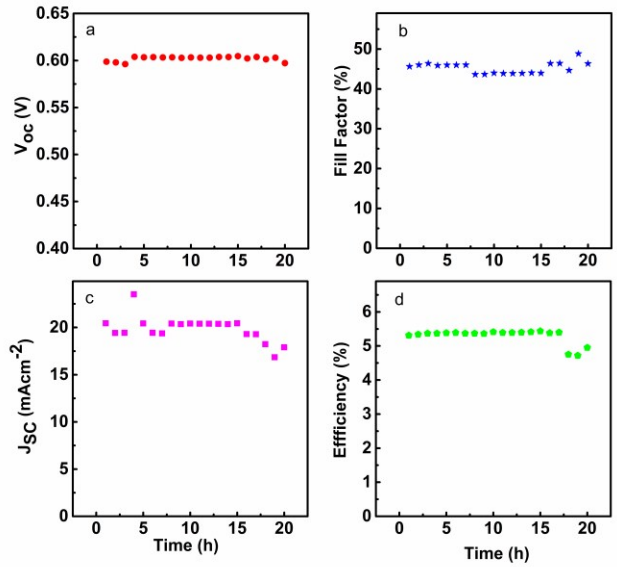

Figure 8: Comparison of I-V parameters variation with aging time for the QDSSC assembled with CE60: (a) open circuit voltage (b) fill factor (c) short current density (d) efficiency

For the best performing QDSSc, stability test was conducted by exposing the cell for 20 continuous hours under light illumination and presented in figure 8. It is found that the cell showed consistent photoconversion efficiency with minimum decrement of only 2.1% in the efficiency. The photoconversion efficiency was found to increase after sufficient exposure to the light illumination since the heating of the electrolyte improves the ionic mobility with good penetration of the electrolyte in to the pores of TiO_2 because of capillary effect.[43,44] Therfore $Cu_{1.8}S$ can be a suitable cost-effective substitute to Pt as counter electrode material with superior electrocatalytic property, high stability and commendable longevity.

4. Conclusion

Stacked nanoplatelets of $Cu_{1.8}S$ were synthesized using CTAB as surfactant. CTAB is found to influence the surface morphology of the $Cu_{1.8}S$ thin films and yields highly crystalline $Cu_{1.8}S$. The electrocatalytic behavior of the $Cu_{1.8}S$ CEs is greatly influenced by the surface morphology and surface active sulfide species. All the QDSSCs assembled $Cu_{1.8}S$ CEs exhibit over 3.87 % of photoconversion efficiency and highest photoconversion efficiency of 5.16% is achieved for the film synthesized at 60 ^{O}C with very low R_S, R_{CT}, R_{CE} and Z_W values and zero corrosion potential against the poor electrocatalytic behavior of Pt owing to catalytic poisoning. The free carrier concentration due to Cu vacancy and the Cu-S bonding at the surface of the counter electrode found to play key role in redox reaction. The electrocatalytic feature of $Cu_{1.8}S$ makes it a suitable cost-effective alternate to Pt as counter electrode.

Author Information

Corresponding Author

*prabakar@pusan.ac.kr, *kprabakar@gmail.com

Conflict of Interest

The authors declare no competing financial interests.

Acknowledgements

This work was supported for two years by the Pusan National University research grant.

References

1. C. Lin, C. Teng, T. Li, Y. Lee and H. Teng, *J. Mater. Chem. A,* 2013, **1**, 1155-1162.
2. I. Mora-Sero, S. Gimaenez, F. Fabregat-Santiago, R. Gomez, Q. Shen, T. Toyoda and J. Bisquert, *Acc. Chem. Res.,* 2009, **42**, 1848-1857.
3. S. Buhbut, S. Itzhakov, E. Tauber, M. Shalom, I. Hod, T. Geiger, Y. Garini, D. Oron and A. Zaban, *ACS Nano,* 2010, **4**, 1293-1298.
4. L. M. Peter, K. G. U. Wijayantha, D. J. Riley and J. P. Waggett, *J Phys Chem B,* 2003, **107**, 8378-8381 .
5. M. Shalom, I. Hod, Z. Tachan, S. Buhbut, S. Tirosh and A. Zaban, *Energy Environ. Sci.,* 2011, **4**, 1874-1878 .
6. W. W. Yu, L. Qu, W. Guo and X. Peng, *Chem. Mater.,* 2003, **15**, 2854-2860.

7. P. Wang, S. M. Zakeeruddin, J. E. Moser, R. Humphry-Baker, P. Comte, V. Aranyos, A. Hagfeldt, M. K. Nazeeruddin and M. Grätzel, *Adv Mater,* 2004, **16**, 1806-1811.
8. R. Vogel, K. Pohl and H. Weller, *Chemical Physics Letters,* 1990, **174**, 241-246.
9. R. Vogel, P. Hoyer and H. Weller, *J. Phys. Chem.,* 1994, **98**, 3183-3188.
10. H. Wang, T. Kubo, J. Nakazaki, T. Kinoshita and H. Segawa, *J. Phys. Chem. Lett.,* 2013, **4**, 2455-2460.
11. L. Li, X. Yang, J. Gao, H. Tian, J. Zhao, A. Hagfeldt and L. Sun, *J. Am. Chem. Soc.,* 2011, **133**, 8458-8460.
12. J. Tian, R. Gao, Q. Zhang, S. Zhang, Y. Li, J. Lan, X. Qu and G. Cao, *J. Phys. Chem. C,* 2012, **116**, 18655-18662.
13. M. Kim, A. Ochirbat and H. J. Lee, *Langmuir,* 2015, **31,** 7609–7615.
14. K. Imoto, K. Takahashi, T. Yamaguchi, T. Komura, J. Nakamura and K. Murata, *Solar Energy Mater. Solar Cells,* 2003, **79**, 459-469.
15. G. Hodes, J. Manassen and D. Cahen, *J. Electrochem. Soc.,* 1980, **127**, 544-549.
16. Y. Lee and Y. Lo, *Advanced Functional Materials,* 2009, **19,** 604-609.
17. A. Banerjee, K. K. Upadhyay, S. Bhatnagar, M. Tathavadekar, U. Bansode, S. Agarkar and S. B. Ogale, *RSC Adv.,* 2014, **4**, 8289-8294.
18. W. J. Lee, E. Ramasamy, D. Y. Lee and J. S. Song, *ACS Appl. Mater. Interfaces,* 2009, **1**, 1145-1149.
19. M. Gao, Y. Xu, J. Jiang and S. Yu, *Chem. Soc. Rev.,* 2013, **42**, 2986-3017.
20. X. Rui, H. Tan and Q. Yan, *Nanoscale,* 2014, **6**, 9889-9924.
21. Y. Hou, D. Wang, X. H. Yang, W. Q. Fang, B. Zhang, H. F. Wang, G. Z. Lu, P. Hu, H. J. Zhao and H. G. Yang, *Nat Commun,* 2013, **4**, 1583.
22. L. Zhang, H. K. Mulmudi, S. K. Batabyal, Y. M. Lam and S. G. Mhaisalkar, *Phys. Chem. Chem. Phys.,* 2012, **14**, 9906-9911.
23. A. Dennyson Savariraj, K. K. Viswanathan and K. Prabakar, Electrochimica Acta 2014, **149**, 364-369.
24. H. Wu and W. Chen, *Nanoscale,* 2011, **3**, 5096-5102.
25. C. Burda, X. Chen, R. Narayanan and M. El-Sayed, *Chem. Rev.,* 2005, **105**, 1025-1102.
26. A. Dennyson Savariraj, K. K. Viswanathan and K. Prabakar, *ACS Appl. Mater. Interfaces,* 2014, **6**, 19702–19709.
27. C. Wu, G. Zhou, D. Mao, Z. Zhang, Y. Wu, W. Wang, L. Luo, L. Wang, Y. Yu, J. Hu, Z. Zhu, Y. Zhang and J. Jie, *Journal of Materials Science & Technology,* 2013, **29**, 1047-1052.
28. M. Saranya, C. Santhosh, R. Ramachandran, P. Kollu, P. Saravanan, M. Vinoba, S. K. Jeong and A. N. Grace, *Powder Technol,* 2014, **252,** 25-32.
29. Q. Lu, F. Gao and D. Zhao, *Nano Lett.,* 2002, **2**, 725-728.
30. J. M. Luther, P. K. Jain, T. Ewers and A. P. Alivisatos, *Nat Mater,* 2011, **10**, 361-366.
31. I. Kriegel, C. Jiang, J. Rodriguez-Fernandez, R. D. Schaller, D. V. Talapin, E. da Como and J. Feldmann, *J. Am. Chem. Soc.,* 2012, **134**, 1583-1590.
32. D. Dorfs, T. Hartling, K. Miszta, N. C. Bigall, M. R. Kim, A. Genovese, A. Falqui, M. Povia and L. Manna, *J. Am. Chem. Soc.,* 2011, **133**, 11175-11180.
33. D. Dorfs, T. Hartling, K. Miszta, N. C. Bigall, M. R. Kim, A. Genovese, A. Falqui, M. Povia and L. Manna, *J. Am. Chem. Soc.,* 2011, **133**, 11175-11180.
34. Y. Liu and C. Z. Huang, *Nanoscale,* 2013, **5**, 7458-7466.
35. R.St.C. Smart, W.M. Skinner and A.R. Gerson, *Suf. Interface Anal.* 1999, **28**, 101-105.
36. K. Laajalehto, I. Kartio and P. Nowak, *Appl. Surf. Sci.,* 1994, **81**, 11-15.
37. Y. Lu, X. Meng, G. Yi and J. Jia, *J. Colloid Interface Sci.,* 2011, **356,** 726-733.
38. Z. Yang, C. Chen, C. Liu and H. Chang, *Chem. Commun.,* 2010, **46**, 5485-5487.
39. J. G. Radich, R. Dwyer and P. V. Kamat, *J. Phys. Chem. Lett.,* 2011, **2,** 2453-2460.
40. V. A. Sethuraman and J. W. Weidner, *Electrochim. Acta,* 2010, **55**, 5683-5694.
41. F. Xie, Z. Shao, G. Zhang, J. Zhai, W. Lu, X. Qin, W. Li and B. Yi, *Electrochim. Acta,* 2012, **67**, 50-54.
42. X. Feng, K. Shankar, M. Paulose and C. A. Grimes, *Angewandte Chemie International Edition,* 2009, **48**, 8095-8098.
43. K. Zhao, H. Yu, H. Zhang and X. Zhong, *J. Phys. Chem. C,* 2014, **118,** 5683-5690.
44. H. McDaniel, N. Fuke, N. S. Makarov, J. M. Pietryga and V. I. Klimov, *Nat Commun,* 2013, **4** :2887.

Table of Contents